Probabilistic forensic assessment of a collapsed concrete grandstand element under a jumping crowd load

H.J.J. Weijs [1], R.D.J.M. Steenbergen [1, 2], M.A.N. Hendriks [3]

[1] TNO Mobility and Built Environment, Reliable Structures, the Netherlands
[2] Ghent University, Faculty of Engineering and Architecture, Belgium
[3] Delft University of Technology, Faculty of Engineering Structures, the Netherlands

On the 17th of October 2021, a concrete grandstand element collapsed at the Goffert football stadium in the Netherlands under a jumping crowd load. In this paper the cause for the collapse is investigated from a probabilistic point of view. Various investigations raised some belief that the actual loads were larger than the design loads for the grandstand elements, also questioning the general reliability of these elements. There are also indications towards construction errors. This paper presents a full probabilistic method to determine the failure probability of the collapsed element in the Goffert stadium, subjected to dynamical crowd loads. Suitable distribution types and parameters of stochastic variables related to forces generated by jumping are derived. Randomly generated excitation signals are created that are used to excite the structure, which is modelled as a non-linear single-degree-of-freedom system with a bi-linear force-displacement relationship. A Monte Carlo simulation shows that 0 of about 10^5 simulations lead to failure of the structure under the crowd loading present during the collapse, if we would model it according to the design drawings. This result makes it unrealistic that the actual loads were higher than the design loads or that the design is unsafe since then we would expect a relatively large failure probability. In situ inspection of the concrete cover on other elements in the stadium show that large variation exists in this parameter, suggesting that the collapsed element could have had a large cover, which reduced its capacity. A sensitivity analysis concludes that the post-yielding stiffness highly influences the failure probability of the grandstand element. These two points combined make it more plausible that the element failed because the actual resistance of the structure was weaker than intended by the design drawings.

Key words: Structural reliability, forensic engineering, jumping loads, concrete grandstand elements, non-linear dynamical analysis

1 Introduction

This paper presents a method to probabilistically determine the failure cause of a concrete grandstand element which is subjected to dynamical crowd loads. Cause for this study is the collapse of an element in the Goffert stadium. At the time of the collapse 93 people were standing on the element. Luckily nobody got injured, but it resulted in an uproar in the Dutch media nevertheless. In the current paper a probabilistic model is derived for both the dynamic crowd load as for the resistance of the concrete element which enables us to draw realistic conclusions about the failure case.

2 Literature overview

In this section an overview of the models for jumping crowd loads are given. A difference is made between analytical models and measurement data. Special attention will be given to possibility of probabilistic quantification. Since only the number of persons on the collapsed element is known from photos (n = 93) , for the other parameters describing the dynamic effects we need accurate probabilistic models.

2.1 An introduction to loads induced by jumping

When a person jumps on a body, they generate a force on it. Figure 2.1 visualizes this in a schematized manner. A person can be schematized as a point mass with mass m and spring stiffness k. During the landing and the offset of a jumping motion, the centre of mass drops, resulting in a compression of the spring. The resulting force follows through

$$F(t) = k\,u(t) \tag{1}$$

where $F(t)$ is the dynamic force of a jump at time t, k is the equivalent spring stiffness of the persons legs and $u(t)$ is the displacement of the point mass at time t.
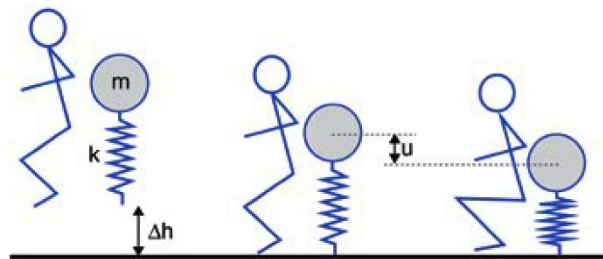

Figure 2.1 A schematization of a person jumping on a rigid body (image from Spanenburg, 2022)

2.2 *Loads generated on a rigid body by a jumping individual*

The load an individual excites on a structure is usually normalized with respect to that person's static weight.

$$\tilde{F}(t) = \frac{F(t)}{G} \tag{2}$$

where $\tilde{F}(t)$ is the weight normalized load, $F(t)$ is the actual force and G is that person's static weight. For data analysis purposes, the maximum value of each normalized jump is the point of interest, therefore $\tilde{F}(t)$ is often abbreviated to $\tilde{F} = \max\left(\tilde{F}(t)\right)$.

Present load models use Fourier series to describe jumping loads (ISO 10137 (2007), British Standard (1996), Canadian National Building Code (2005), Stichting Bouwresearch (2005)). These models are based on research by Ji & Ellis (1994), who propose the following equation to describe jumping loads

$$F(t) = G\left(1.0 + \sum_{n=1}^{\infty} r_n \sin\left(\frac{2n\pi}{T_p}t + \phi_n\right)\right) \tag{3}$$

where n is the number of the n-th harmonic, r_n is the Fourier coefficient of the n-th harmonic, T_p is the period of the activity (i.e., jump period) and ϕ_n is the phase lag of the n-th harmonic. Ji & Ellis (1994) established a relation between the jump factor and the contact ratio and determined the Fourier coefficients of the first six terms. The contact ratio is defined as

$$\alpha = \frac{t_p}{T_p} \leq 1.0 \tag{4}$$

where α is the contact ratio, t_p is the contact duration between the person and the ground and T_p is the period of the jump. A lower contact ratio means that the airtime is higher, from which analogously follows that the jump factor will be higher. Based on physiology, Bachmann & Ammann (1987) found a lower bound for t_p of 0.15 s. Commonly used contact ratios are $\alpha = \frac{1}{3}$, $\alpha = \frac{1}{2}$, and $\alpha = \frac{2}{3}$, which results in jump factors of $\tilde{F} = 4.8$, $\tilde{F} = 3.2$ and $\tilde{F} = 2.3$, respectively (Ji & Ellis, 1994). Figure 2.2 shows this signal for the three contact ratios at a jumping frequency of 2 Hz.

Sim et al. (2008) showed that a sine-squared function better describes jumping-induced loads than a sine function. Additionally, people will not jump perfectly periodic but with (among others) different jump factors and contact ratios. These phenomena are not

included in Equation 3. This makes the model presented in Equation 4 unsuited to use in an accurate failure probability assessment.

2.3 *Loads generated on a rigid body by a jumping crowd*

Loads generated by a crowd cannot be obtained by simply multiplying the load of an individual by the number of people. The load is attenuated because peaks of everyone's excitation do not align perfectly. Therefore we use a dataset of measured force signals under jumping crowd loads. In Figure 2.3, measured force signals of jumping individuals are presented, clearly showing the difference between perfectly periodic signals (i.e., using Equation 2) and actual signals.
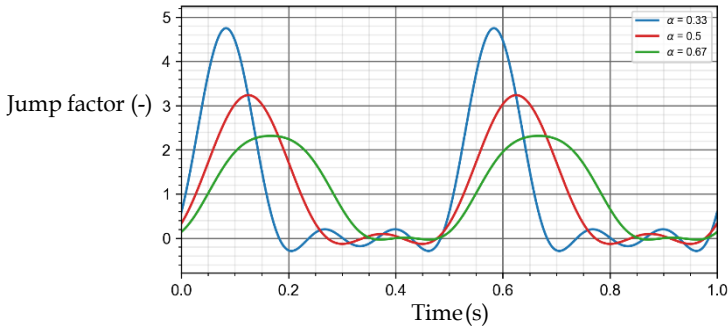

Figure 2.2 Synthetic excitation signal of an individual jumping at 2 Hz
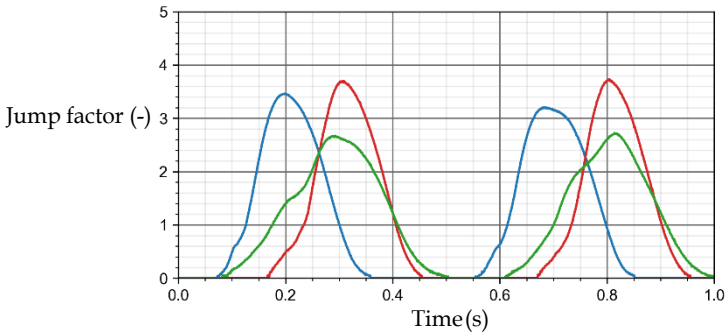*(model from Ji & Ellis, 1994)*

Figure 2.3 Actual excitation signal of three individuals jumping at 2 Hz
(data Xiong & Chen, 2021)

100

An easy and often used method to tackle this phenomenon is by incorporating a coordination factor. This factor reduced the load of a group by accounting for the lack of coordination between individuals. The total excitation signal of a group would then be equal to the excitation signal of an individual (i.e., using Equation 3) multiplied by the number of people and the coordination factor.

Multiple studies agree that the value of the coordination factor depends on the group size (Ebrahimpour & Sack (1989), Ellis & Ji (2004), Chen et al. (2019)). The value of this factor, however, is highly disputed, e.g. Ellis & Ji (2004) report a value of around 0.6, while Chen et al. (2019) found a factor of 0.9.

A consequence of using Equation 3, combined with a coordination factor is that the total excitation signal is a perfect periodic function. In a dynamical analysis, the harmonics of this function could match one of the eigenfrequencies of the structure, which would result in a resonant response. Brownjohn et al. (2004) have shown that there is some energy leakage to adjacent frequencies when jumping. This leakage becomes more profound for increasing harmonics. A resonant response would therefore be artificial. Preference should be given to randomizing the phase lag between individuals, but scientific substantiation for this variable is not presented yet.

2.4   *Stochastic quantification based on jumping data*

The previous paragraphs have presented present load models for jumping individuals and crowds, as well as their flaws. Therefore, in this study we prefer to base the assessment on measured signals rather than on models. In Figure 2.4, measurements of excitation signals are presented. These signals are part of a large database, which is the result from work executed by Xiong & Chen (2021). This database contains 334 signals of jumping individuals and 92 signals of jumping crowds, up to 48 people. Figure 4 presents an example of such a signal.

Basing ourselves on the measured data, also stochastic quantification of relevant parameters becomes possible. The next chapter provides the distribution type and parameters related to jumping motions.
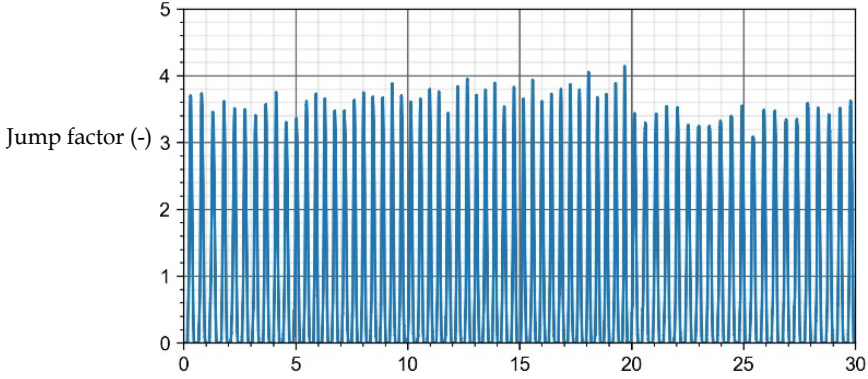
Figure 2.4 Excitation signal of an individual jumping at 2 Hz

(data from Xiong and Chen, 2021)

3   Stochastic quantification of random variables related to jumping

3.1   Jump factor $\tilde{F}$

The jump factor describes the ratio between the dynamic force excited by a jump $F(t)$ and that person's static weight G (see Equation 2). In this assessment, it is assumed to be the sum of two separate variables: (1) one that describes the series-to-series difference between peaks $\tilde{F}_{sts}$ (i.e., the difference between two individuals' average jump factor), and (2) one that describes the difference in peaks within a series $\tilde{F}_{ws}$ (i.e., the difference between subsequent jumps of a single individual):

$$\tilde{F} = \tilde{F}_{sts} + \tilde{F}_{ws} \tag{5}$$

After cleaning the data, 236 out of the 334 are deemed useful. Faulty datasets included non-metronome-guided jumping or too many missed jumps. For each of the 236 remaining excitation signals, the mean value and the standard deviation of the jump factor is determined. The result is shown in Figure 3.1.

Series-to-series jump factor $\tilde{F}_{sts}$

The distribution type and parameters that best describe the series-to-series jump factor, $\tilde{F}_{sts}$, is a normal distribution with the following parameters:

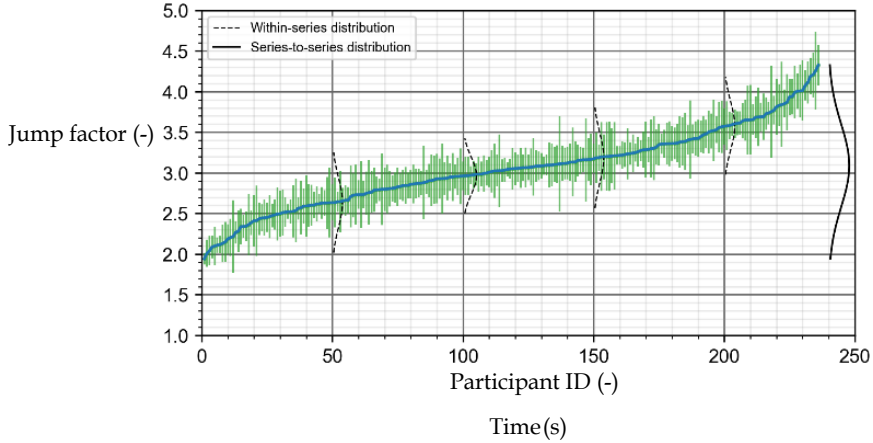$$\tilde{F}_{sts} \sim N(\text{loc} = 3.09, \text{scale} = 0.51)$$

Time (s)

Figure 3.1 Mean value (blue) ± 1 standard deviation (green) of all peaks of the jump factor

Within-series jump factor $\tilde{F}_{ws}$

The distribution type and parameters that best describe the within-series jump factor, $\tilde{F}_{ws}$, is a Weibull distribution with the following parameters:

$$\tilde{F}_{ws} \sim \text{Weib}(\text{shape} = 68.9 \cdot 10^6, \text{loc} = 51.3 \cdot 10^6, \text{scale} = 51.3 \cdot 10^6)$$

No correlation between the series-to-series and within-series jump factors

With the marginal distributions defined, only the correlation between $\tilde{F}_{sts}$ and $\tilde{F}_{ws}$ needs to be defined to fully describe the jump factor $\tilde{F}$. Correlation between two random samples X and Y can be determined through

$$\rho_{x,y} = \frac{\sum_{i=1}^{n}(x_i - \overline{x})(y_i - \overline{y})}{\sqrt{\sum_{i=1}^{n}(x_i - \overline{x})^2 \sum_{i=1}^{n}(y_i - \overline{y})^2}} \tag{5}$$

where $\rho_{x,y}$ is the Pierson correlation coefficient, n is the sample size, x_i, y_i are the sampled points of random variables X and Y, and $\overline{x}, \overline{y}$ are the sampled means of variable X and Y. The resulting correlation coefficient is 0.20, indicating low correlation. In modelling the jump factor $\tilde{F}$, the two variables are therefore assumed to be uncorrelated.

The jump factor from the data set shows similar results to values that the literature describe.

3.2   *Contact ratio α*

The contact ratio is the contact duration between the person and the ground, relative to the jump period (see Equation 4). For each participant, the average contact ratio is determined.

The distribution type and parameters that best describe the contact ratio α is a normal distribution with the following parameters:

$$\alpha \sim N(\text{loc} = 0.66, \text{scale} = 0.08)$$

According to the data set, the expected value of the contact ratio is 0.66. When compared to literature (e.g. Ellis et al, 2000), this is on the high side. The origin of this difference is not investigated. A possible explanation could be that these studies base their results on mathematical models instead of a data set, which might correctly estimate the jump factor, but underestimates the contact ratio. To prevent too lenient results, the expected value of the contact ratio is chosen to be in line with what is found in literature. This is a conservative approach.

$$\alpha \sim N(\text{loc} = 0.33, \text{scale} = 0.08)$$

3.3 Correlation between the jump factor $\tilde{F}$ and the contact ratio α

Section 2.2 mentioned the negative relation that exists between the jump factor and the contact ratio. In Figure 3.2 the relation between $\tilde{F}_{sts}$ and α and between $\tilde{F}_{ws}$ and α are illustrated, respectively. The Pierson correlation coefficients are included in the figure. The figure clearly illustrated the correlation between $\tilde{F}_{sts}$ and α and therefore it needs to be included when generating an excitation signal. The correlation between $\tilde{F}_{ws}$ and α is so low that it can be ignored.
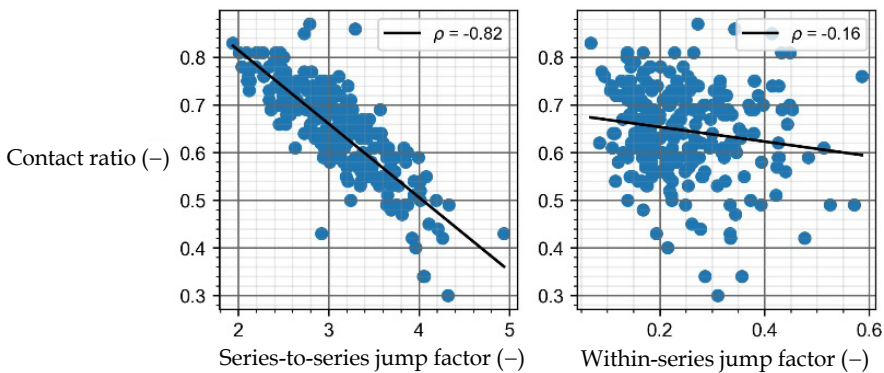

Figure 3.2 Correlation analysis between the contact ratio and the series-to-series jump factor, and within-series jump factor, respectively

3.4 *Autocorrelation*

Autocorrelation measures the dependence of a variable with a lagged version of itself. In this study the lag follows from a time difference between subsequent jumps. The autocorrelation function for both the jump factor $\tilde{F}$ and the contact ratio α are examined. Because the peak values resulting from the data set are a realization of the series-to-series jump factor and the within-series jump factor, it is only possible to determine the autocorrelation function for the combination of the two variables.

Figure 3.3 presents the temporal autocorrelation functions of $\tilde{F}$ and α, respectively, for the first 10 lags. Both variables show a quick, steep drop in autocorrelation.

Although both are so low that autocorrelation could be neglected, the first lag is considered. The autocorrelation for the jump factor is $\rho_{\tilde{F}_i,\tilde{F}_{i+1}} = 0.28$. For the contact ratio this value is $\rho_{\alpha_i,\alpha_{i+1}} = 0.20$.
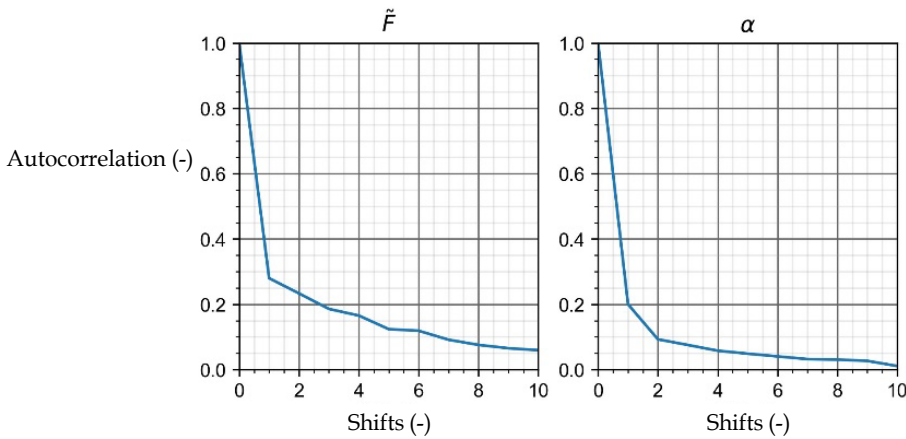

Figure 3.3 Temporal autocorrelation functions for the jump factor and the contact ratio

3.5 *Jump period T_p*

The jump period describes the duration of a single jump. The period at time i, (i.e. $T_{p,i}$) depends on the previous $i - 1$ realisations (Ellis & Ji (2004), Sim et al. (2008)). Literature has shown that currently no equivocal distribution type and parameters exist for T_p. Evaluation of the data set shows that the coefficient of variation of the jumping period is 0.10 at 2 Hz. For larger frequencies, the value tends to converge to 0.08. A coefficient of variation of 0.10 means that the standard deviation of a 2 Hz guided jump is 0.05 s.

Because of the disagreements in literature, a safer value for the standard deviation is chosen: 0.02. This is a conservative approach.

The distribution type and parameters that best describe the jump period, T_p, is a normal distribution with the following parameters:

$$T_{p,n} \sim N(\text{loc} = \sum_{i=1}^{n} (n \cdot \mu - T_{p,i}), \text{scale} = 0.02)$$

where μ is the mean value of the jump period.

3.6   Phase lag ϕ

The phase lag represents the natural difference in timing between individuals. No conclusive literature was found on the distribution type and parameters of this variable. Therefore, the phase lag ϕ is assumed to be modelled as a normal distribution with the following parameters:

$$\phi \sim N(\text{loc} = 0, \text{scale} = 0.05)$$

3.7   Overview of the parameters

Tables 3.1-3.3 present the variables that are used to generate normalized excitation signals. In order to create a single excitation signal, the normalized excitation signal needs to be multiplied with a static weight $G = mg$, where m is the mass of a person. To create excitation signals for a group of size n, this process needs to be repeated n times. The differences in the jump period T_p, the contact ratio α and the phase lag ϕ ensure that a narrow banded signal is created.

Table 3.1. Stochastic quantification of variables relevant to the generation of excitation signals

Variable		Distribution type
Jump factor (between series)	$\tilde{F}_{sts}$	Normal (loc = 3.09, scale = 0.51)
Jump factor (within series)	$\tilde{F}_{ws}$	Weibull (k = 68.9·10⁶, loc = 51.3·10⁶, scale = 51.3·10⁶)
Contact ratio	α	Normal(loc = 0.33, scale = 0.08)
Jump period	T_p	Normal(loc = T_p, scale = 0.02)
Phase lag	ϕ	Normal(loc = 0, scale = 0.05)

Table 3.2 Correlation table

	$\tilde{F}_{sts}$	$\tilde{F}_{ws}$	α
$\tilde{F}_{sts}$	1	0	-0.82
$\tilde{F}_{ws}$	0	1	0
α	-0.82	0	1

Table 3.3 Temporal autocorrelation table

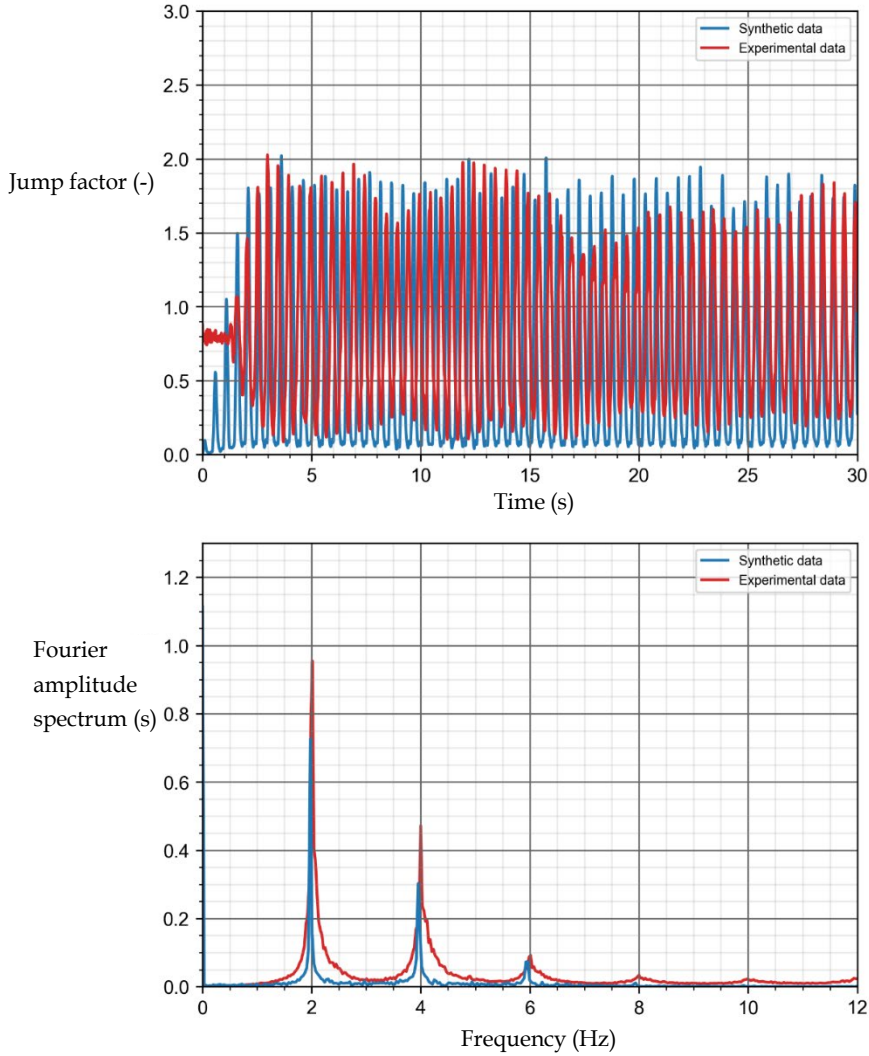|	$\tilde{F}_i$	α_i
$\tilde{F}_{i+1}$	0.28	-
α_{i+1}	-	0.20

Figure 3.4 A random realisation of the synthetically generated and an experimentally obtained excitation signal

Figure 3.4 presents a random realisation of the excitation signal and a randomly picked signal from the experiments, both with an excitation frequency of 2 Hz. In the time domain, the results look quite similar. The frequency domain shows larger contributions around the harmonics in the experimental data compared to the synthetic data.
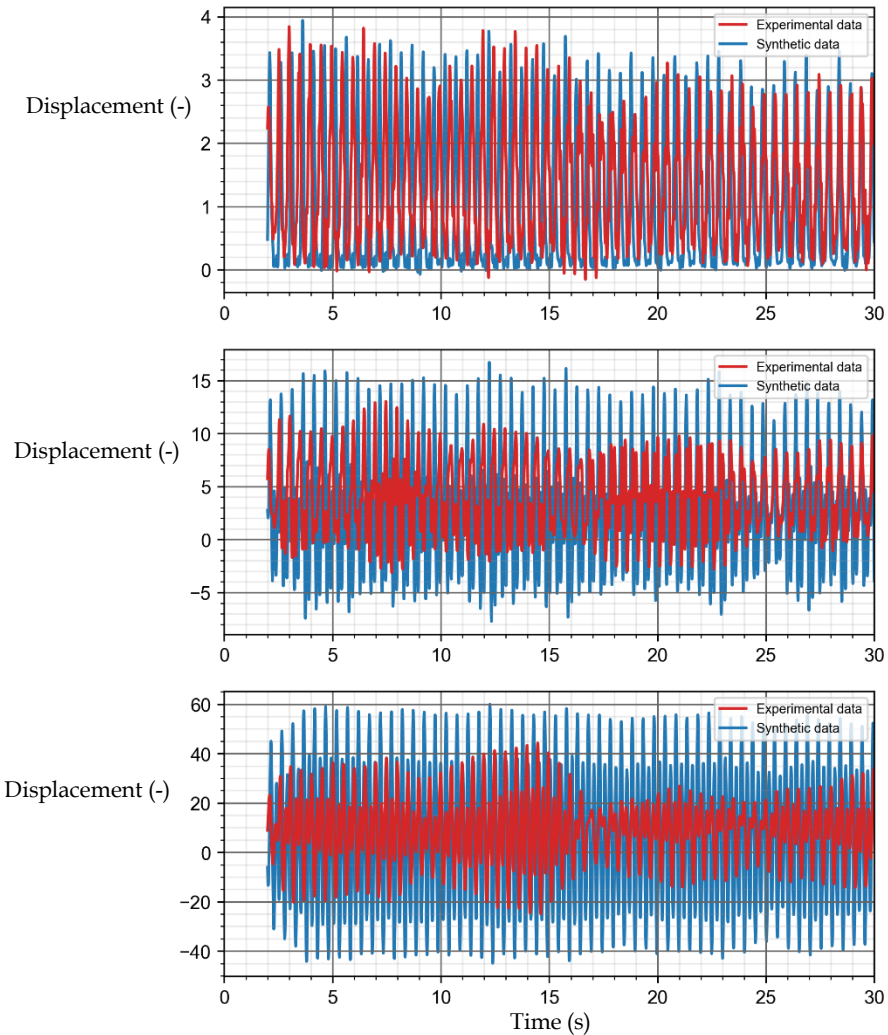

Figure 3.5 Linear elastic response of a system to an experimentally obtained (red) and synthetically generated (blue) excitation signal. The structure's natural frequency is 10 Hz (top), 6 Hz (middle) or 4 Hz (bottom).

To compare the effects of the different load signals the linear elastic response is computed for three systems with natural frequencies equal to f_e = 10 Hz, 6 Hz and 4 Hz, see Figure 3.5. As can be depicted from this figure, the result is that for decreasing natural frequencies, the displacement is overestimated. Based on that it seems that the synthetic excitation signals lead to an overestimate of the structural response. It is not investigated if this conclusion can be drawn in general or of this if it is related to this specific outcome.

4   Method

4.1   *The dynamical system*

A non-linear dynamical system is introduced to describe the behaviour of the grandstand element. If human-structure interaction (HIS) is ignored, the element can be modelled as a single degree of freedom (SDOF) system (Ellis et al., 2000). Inclusion of HIS, leads to a reduced response for individuals jumping (Shahabpoor & Pavic (2016), Yao et al. (2002), Gaspar et al. (2020). However, a study on the interaction between groups and a structure show that the net reduction is negligible for lightweight structures (Appelman, 2022). No literature was found that describes the influence of HSI of a group on a heavier structure was found. Further research in this matter is required. For now, HSI is ignored in this dynamical system.

The non-linear spring in the dynamical system is characterized by a force-displacement relationship, which describes its behaviour up to the point of failure. A bi-linear force-displacement relationship with strength hardening is adopted (see Figure 4). To include the non-linear region in the analysis, the design criteria change from the usual strength-
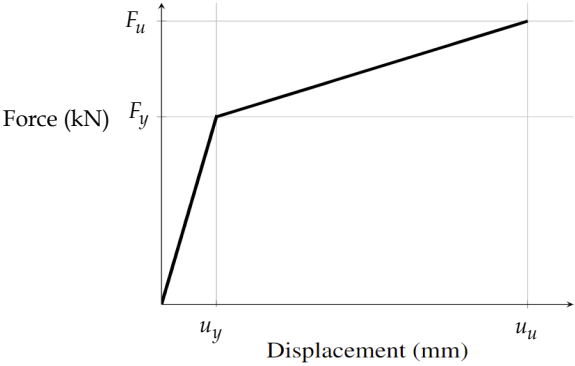

Figure 4.1 A bilinear force-displacement relationship

The subscripts y and u indicate the yield- and failure point of the structure

basis to a displacement-basis, where the ultimate displacement u_u cannot be exceeded. This is a commonly used design criterion in e.g. seismic design (Tsouvalas 2020), but it can also be applied to this analysis.

For each dynamical system an equation of motion (EOM) needs to be derived to describe its behaviour. The EOM of a non-linear SDOF is given as (Tsouvalas 2020)

$$m\frac{\partial^2 u}{\partial t^2} + c\frac{\partial u}{\partial t} + f_s\left(u, \text{sgn}\left(\frac{\partial u}{\partial t}\right)\right) = F(t) \tag{6}$$

where m, c and k are the mass, the viscous damping, and the stiffness of the system, respectively, u is the midspan displacement of the system, $\frac{\partial}{\partial t}$ indicates a derivative with respect to time, $f_s(\ )$ is the restoring force of the system, sgn($\ $) is the signum function (which returns -1 for arguments smaller than 0, returns 0 if the argument is 0, and returns $+1$ for arguments larger than 0), and $F(t)$ is the force in the system. Figure 5 presents the equivalent mass-damper-spring system of the concrete grandstand element. The restoring force (i.e. $f_s(\ )$) is modelled as a parallel combination of a linear spring and a hysteretic spring.
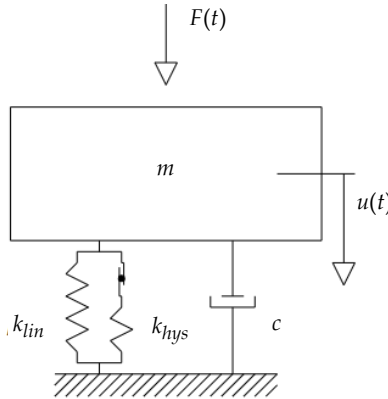
Figure 4.2 The equivalent mass-damper-spring system of the concrete grandstand element

The restoring force stores all inelastic characteristics that the system has in it (Tsouvalas 2020). In this system the non-linear behaviour of the restoring force is based on two phenomena: (1) strength hardening, and (2) hysteresis. Strength hardening means that the post-yielding stiffness has a positive value, which is depicted in Figure 4.1. Hysteresis indicates that there is a delay between the input and the output of a system. In structural dynamics, hysteresis loops are found when comparing the force exciting the system (input)

with the displacement (output). The displacement lags the force, ensuring that loops are formed. Each enclosed loop is equal to the energy dissipation of the system.

Sivalsevan & Reinhorn (1999) propose the following equation to model a hysteretic spring

$$k_{hys} = (1 - r_k)k_0 \left(1 - \left| \frac{F^*}{F_y^*} \right|^N \left(\eta_1 \text{sgn} \left(F^* \frac{\partial u}{\partial t} \right) + \eta_2 \right) \right) \tag{7}$$

where r_k is the ratio between the elastic and the post-yielding stiffness, k_0 is the eastic stiffness of the system, F^* is the portion of applied force shared by the hysteretic spring, F_y^* is the yield force of the hysteretic spring, N is a parameter controlling the smoothness of the transition from elastic to inelastic, η_1 is a parameter controlling the shape of the unloading curve ($0 < \eta_1 < 1$), and $\eta_2 = 1 - \eta_1$. This yields a combined stiffness of:

$$k_{sys} = k_{lin} + k_{hys} = r_k k_0 + (1 - r_k)k_0 \left(1 - \left| \frac{F^*}{F_y^*} \right|^N \left(\eta_1 \text{sgn} \left(F^* \frac{\partial u}{\partial t} \right) + \eta_2 \right) \right) \tag{8}$$

4.2 *The reliability analysis*

Failure of a structure is described by introducing a limit state function (LSF)

$$Z(u,t) = R(u) - S(\ddot{u},t) \tag{9}$$

where $Z(u,t)$ is the limit state function, $R(u)$ is the resistance function and $S(\ddot{u},t)$ is the solicitation function. Failure occurs in the region where the solicitation is larger than the resistance, i.e., when $Z < 0$. The design criterion of this non-linear dynamical system is displacement based, making the limit state function a function of both displacement and time. The solicitation function $S(\ddot{u},t)$ is equal to the excitation a crowd induces on the element. The resistance function $R(u)$ is described using a bi-linear force-displacement relationship.

The solicitation function $S(\ddot{u},t)$ is constructed by using the stochastic variables, mentioned in Tables 3.1-3.3. The normalized ground reaction forces are translated to an acceleration through (Racic et al., 2010)

$$\tilde{F}(t) = \ddot{u}(t)/g + 1 \tag{10}$$

where g is the gravitational acceleration constant. This is done for every individual. The total excitation signal is the superposition of each individual's signal, multiplied with an

influence factor that corrects for each person's location at the grandstand. As the database of Xiong & Chen (2021) consists of 30-second excitation signals, the artificially generated signals are also 30 seconds.

It is assumed that crowds are uniformly distributed, which is a reasonable take (Ellis & Ji, 2002). The influence factor is determined using The Maxwell-Betti reciprocal work theorem. The Maxwell-Betti reciprocal work theorem states that the influence line of the displacement at midspan of a structure, given the spatial coordinate of the unity load, is equal to the displacement line of the structure, given a midspan unity load. Under the assumption that the grandstand element can be modelled as a simply supported, slender beam with a constant bending stiffness, the displacement of the structure given a midspan load is obtained using the Euler-Bernoulli beam theory

$$\frac{\partial^2}{\partial x^2}\left(EI\frac{\partial^2 u(x)}{dx^2}\right) = q(x) \tag{11}$$

where EI is the bending stiffness of the structure, $u(x)$ is the displacement of the structure at position x $(0 < x < L)$, and $q(x)$ is the applied lateral load at position x.

For the resistance function $R(u)$ we use the finite element model presented in (Royal HaskoningDHV, 2022). This yields a deterministic parameter. Therefore, a model uncertainty parameter θ is introduced. Failure of concrete beams due to the yielding of the reinforcement steel shows a coefficient of variation of around 5% (Schlune et al. (2012), Casas et al. (2007). These findings are based on static analyses, however. No literature was found regarding a model uncertainty factor of concrete structures subjected to dynamical analysis. To account for this uncertainty, the coefficient of variation is doubled to 10%. Future studies should verify this assumption. No bias is expected in the numerically obtained resistance. Therefore a normal distribution with a mean value of $\mu = 1$ is proposed to account for the model uncertainty

$$R(u) = \theta\, R_{\mathrm{nm}}(u) \tag{12}$$

where $\theta \sim N(1, 0.1^2)$ is the model uncertainty parameter, and $R_{\mathrm{nm}}(u)$ is the numerically obtained force-displacement relationship. Because degradation effects are neglected in this study, the resistance function is independent of time.

A Monte Carlo simulation is proposed to determine the reliability, due to the complexity of the analysis (i.e., non-linear and dynamical). This is a type III reliability method, indicating that it can be deployed to determine the true probability of failure. Monte Carlo relies on repeated random sampling over many experiments. Each simulation has its own unique set of randomly sampled variables. Therefore, each outcome is different.

The outcome of each analysis are two values: (1) a maximum structure displacement u_{max}, resulting from the solicitation function $S(\ddot{u}, t)$, and an ultimate displacement u_u, which follows from the resistance function $R(u)$. If the structure's maximum displacement exceeds its ultimate displacement, the structure is considered to have failed (see Equation 9, where Z becomes smaller than 0). The probability of failure follows from the ratio of failed number of experiments n_f over the total number of experiments n

$$P_f = \frac{n_f}{n} \tag{13}$$

4.3 The collapsed element in the Goffert stadium

In this section a probabilistic forensic assessment is performed to the collapsed element in the Goffert stadium. Table 4.1 presents the parameters that are used in the probabilistic forensic assessment. The grandstand element collapsed in reality after about 8 seconds of rhythmic jumping at 2 Hz. At the moment of collapse, 93 people were present on the grandstand element, divided over 3 rows. The structure broke in two, with a break line in the middle. This indicates that its bending moment capacity was exceeded. Section 4.2 explained how the location dependent influence factors are determined. They are shown in Table 4.2. Because of geometrical symmetry of the beam, only the first half of the influence factor is presented. The number of people on these locations are doubled (i.e., 6 people instead of 3). Their excitation signals are still unique, though. The multiplication at location x_i is assumed to be equal to the ratio between the displacement at that location, w_{x_i} and the maximum displacement of the beam, w_{max}.

The ultimate bending capacity of a concrete structure is linearly related to the internal lever arm between the centre of the concrete compressive zone and the location of the reinforcement steel. The collapsed element had a thickness of 120 mm, which means that the internal lever arm is somewhere in the range of 95 mm (assuming $z = 0.8h$, where z is the internal lever arm, and h is the thickness of the beam). Small deviations in the concrete cover could result in significant changes in the ultimate bending capacity. In the FEM

analysis, a concrete cover of 40 mm was applied based on the design drawings. The FEM analysis is performed to determine the structural capacity of the grandstand element. No measurements of the collapsed element are shared in (Royal HaskoningDHV, 2020), thus it is not possible to determine if the collapsed structure might have been subjected to a

Table 4.1 Assessment parameters

Load parameters	Symbol	Value	Units	Reference
Number of people	n	93	-	1
Mass of a person	m_p	85	kg	2
Gravity constant	g	9.81	m/s^2	2
Grandstand structural properties				
Mass	m_G	$14.2 \cdot 10^3$	kg	1
Yield strength	F_y	$249 \cdot 10^3$	N	1
Yield displacement	u_y	$6 \cdot 10^{-3}$	m	1
Elastic stiffness	k_0	$41.5 \cdot 10^6$	N/m	1
Ultimate strength	F_u	$376 \cdot 10^3$	N	1
Ultimate displacement	u_u	$40 \cdot 10^{-3}$	m	1
Post-yielding stiffness	k_{nl}	$3.74 \cdot 10^6$	N/m	1
Stiffness ratio	r_k	0.09	-	1
Damping properties				
Damping ratio	ζ	0.05	-	1
Stiffness-proportional damping coefficient	α	$1.86 \cdot 10^3$	-	2
Mass-proportional damping coefficient	β	0	-	2
Smoothness parameter	N	10	-	2
Unloading shape parameter	η_1	0.5	-	2
Unloading shape parameter	η_2	0.5	-	2

Reference 1: Royal HaskoningDHV (2022)

Reference 2: For these parameters, no (definite) value could be obtained from Royal HaskoningDHV (2022). Multiple masses are used throughout the study, of which 85 kg is the heaviest. Structural damping in the system is modelled as Rayleigh damping, where all damping is assumed to result from the stiffness-proportional damping coefficient. The smoothness parameter N and the parameters that control the shape of the unloading curve, η_1 and η_2 are taken such that energy dissipation by hysteresis is insignificantly small.

lower than intended internal lever arm. However, concrete cover measurements on 23 other elements in the stadium have been shared in the same report, see Table 4.3. These measurements show large deviations in the concrete cover at midspan. Of all these measurements the average minimum, mean and maximum concrete cover is measured. When taking the average of the largest concrete covers, this value is 16 mm larger than its mean value. With an element thickness of 120 mm, a loss of internal lever arm of 16 mm would prove very significant.

Higher concrete covers result in a lower internal lever arm, reducing the ultimate bending moment capacity of the structure. Up until the yielding point of the reinforcement steel, the structure is assumed to be uninfluenced by this, because the concrete tensile strength is largely responsible for the pre-yielding stiffness. This characteristic is unaffected by a change in the concrete cover.

Table 4.2 Location dependent load multiplication factors

Number of people	x (m)	$w(x)/EI$	Influence factor
6	0.00	0.00	0.000
6	0.28	1.28	0.100
6	0.57	2.54	0.199
6	0.85	3.79	0.296
6	1.13	5.00	0.397
6	1.42	6.16	0.481
6	1.70	7.27	0.568
6	1.98	8.31	0.649
6	2.27	9.26	0.724
6	2.55	10.13	0.792
6	2.83	10.90	0.852
6	3.12	11.55	0.903
6	3.40	12.08	0.944
6	3.68	12.47	0.975
6	3.97	12.71	0.993
3	4.24	12.79	1.000

$\Sigma = 93$

Table 4.3 Minimum, average and maximum measured concrete cover on other grandstand elements in the Goffert stadium (Royal HaskoningDHV, 2022)

Element type	Measured concrete cover (mm)			Minimum and maximum deviation			
	min	average	max	(mm)	(%)	(mm)	(%)
1	41	52	72	20	38	-11	-21
2	42	48	60	12	25	-6	-13
2a	33	43	65	22	51	-10	-23
3	41	46	52	6	13	-5	-11
4	44	57	72	15	26	-13	-23
5	38	58	83	25	43	-20	-34
6	33	41	69	28	68	-8	-20
8	25	41	59	18	44	-16	-39
9	27	34	48	14	41	-7	-21
10s	26	38	54	16	42	-12	-32
11s	21	37	56	19	51	-16	-43
13s	26	36	47	11	31	-10	-28
14s	21	34	62	28	82	-13	-38
15	34	39	58	19	49	-5	-13
16	32	41	55	14	34	-9	-22
17	27	34	39	5	15	-7	-21
18	24	34	69	35	103	-10	-29
19	19	38	54	16	42	-19	-50
20	29	38	51	13	34	-9	-24
21	24	34	49	15	44	-10	-29
22	25	28	34	6	21	-3	-11
23	33	36	49	13	36	-3	-8
24	38	41	45	5	10	-3	-7
		Average deviation		16	41	-10	-24
		Extreme deviation		35	103	-19	-50

A sensitivity study on the structure is performed in which the post-yielding stiffness is reduced. In total, two sensitivity studies are performed where the non-linear resistance is reduced by 10% and 20%, respectively. The values of the yield- and ultimate points can be found in Table 4.4, whereas Figure 4.3 shows the force-displacement relationships. The actual influence of a different concrete cover on the bending capacity is much more complex and should follow from a non-linear analysis. These values therefore no longer represent the actual structure: they are chosen to demonstrate the influence the post-yielding stiffness has on the probability of failure.

Table 4.4 Calculation parameters used for the weakened force-displacement relationship

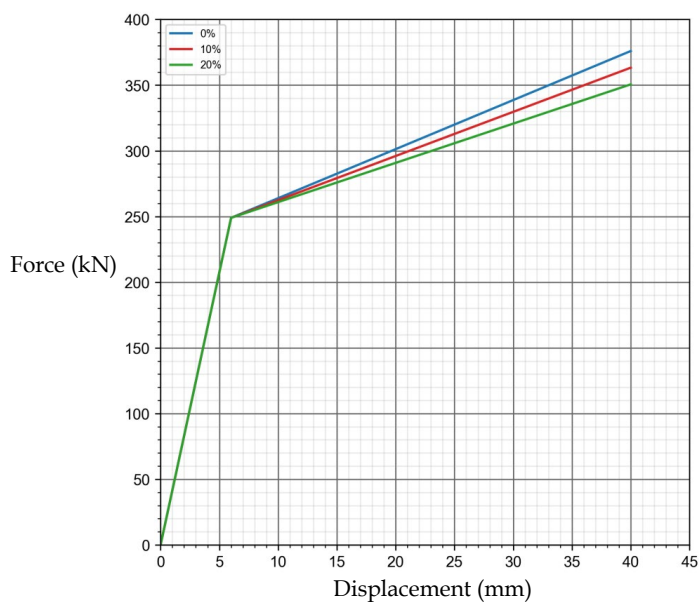| Weakened	u_y (m)	F_y (N)	u_u (m)	F_u (N)
0%	$6 \cdot 10^{-3}$	$249 \cdot 10^3$	$40 \cdot 10^{-3}$	$376 \cdot 10^3$
10%	$6 \cdot 10^{-3}$	$249 \cdot 10^3$	$40 \cdot 10^{-3}$	$363.3 \cdot 10^3$
20%	$6 \cdot 10^{-3}$	$249 \cdot 10^3$	$40 \cdot 10^{-3}$	$350.6 \cdot 10^3$

Figure 4.3 Weakened force-displacement relationship used in the probabilistic forensic assessment

5   Results and discussion

This section presents the results of the study. A total of 94,221 randomly generated excitation signals of 93 people jumping at 2 Hz were created. The routine generates excitation signals of 30 seconds, whereas the actual structure collapsed after about 8 seconds. Thus, the signals have a significant duration: if failure happens within 8 seconds, it also happens within 30 seconds, but if failure happens within 30 seconds, it does necessarily happen within 8 seconds. The presented failure probabilities are therefore to be interpreted as an upper bound to the real situation.

Figure 6 presents the results of the initial analysis and the two sensitivity analyses. On the horizontal axis unity checks are presented (see Equation 14) in bins with a width of 0.05. The vertical axis shows the height of each bin. The unity check is the ratio the structure's maximum displacement and its ultimate displacement

$$\text{uc} = \frac{u_{max}}{u_u} \tag{14}$$

A unity check larger than 1.0 indicates that Z is smaller than 0, and thus failure. A unity check larger than 1.0 indicates the opposite.

When the post-yielding stiffness conforms the numerically determined stiffness (i.e., 0% reduced), 0 out of the 94,221 simulations failed. A 10% reduction in the post-yielding stiffness results in 6 failed cases out of the 94,221. When the post-yielding stiffness is reduced by 20%, 219 out of the 94,221 simulations failed.

This sensitivity analysis proves that the post-yielding capacity of a structure is a key parameter when investigating the reliability of a grandstand element. With a resistance function based on the design drawings and design loads, 0 out of 94,221 simulations failed after 30 seconds of jumping. In reality, 1 out of 30-40 elements failed after 8 seconds. A high discrepancy is found between the failure probability of the actual structure and the failure probability of the structure based on the design drawings. If the structure was built as based on the design drawings, it fails to explain the true probability of failure of this system: a much higher probability of failure is to be expected. This indicates that either the model or the input was incorrect.
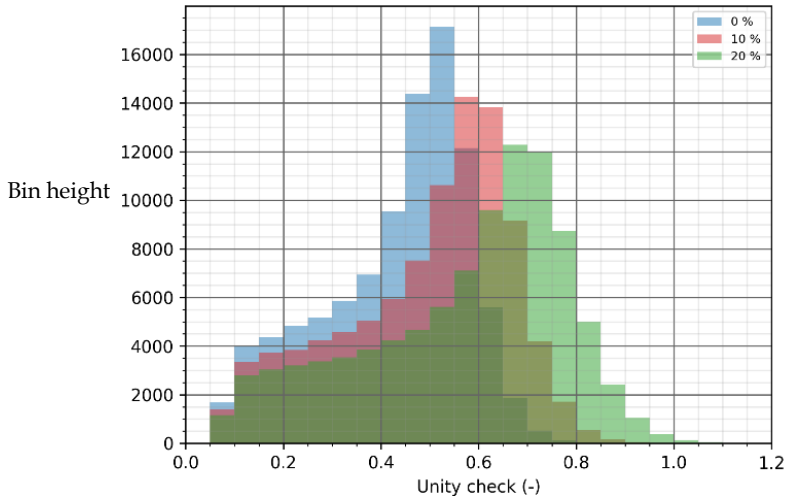
118

Figure 5.1 The resulting unity checks for each simulation for the structure with a 0%, 10%, and 20% reduced post-yielding stiffness

The proposed dynamical system is a commonly used method to model a grandstand element. The dynamical system is therefore judged to lead to unbiased results for this analysis.

The excitation signals are state of the art. They are generated such that they describe the jumping behaviour of a crowd as accurately as possible. Stochastic variables were determined, and the excitation signals were randomly sampled. There is no reason to assume that the database that was used to determine the stochastic variables is unreliable, therefore there is also no reason to assume the excitation signals are unreliable.

The coefficient of variation of the resistance uncertainty parameter θ is assumed to be 10%. 5% could be linked to tests performed on failure of concrete beams where failure occurred as a result of the yielding of steel. The influence of the dynamical basis of this analysis stond could not be expressed in terms of an additional coefficient of variation that was based on literature. Therefore, the choice was made to double the uncertainty. This assumption is not unreasonable.

The force-displacement relationship based on the technical drawings presented in (Royal HaskoningDHV, 2020) is determined using generally accepted software was used in their analyses. There is no reason to assume that the force-displacement relationship based on the technical drawings was wrongly determined by (Royal HaskoningDHV, 2020).

Although no measurements of the concrete cover of the collapsed element were shared, large deviations on other elements were measured. If this were also the case for the collapsed element, it would have been incorrect to assume that the resistance of the structure conforms to the resistance based on the technical drawings. Although it cannot be determined if this element was, in fact, also subjected to large deviations, it is not unreasonable to assume that it was. Additionally, a sensitivity study showed that the post-yielding stiffness, which is linearly related to the internal lever arm between the centre of the concrete compressive force and the location of the reinforcement steel, highly influences the reliability of the structure.

A combination of a proper modelling of the dynamical system, accurately modelled excitation signals and a numerically determined resistance conform the technical drawings fails to explain the observed collapse. The sensitivity study has shown the influence of the non-linear capacity of an element with respect to its reliability index, while concrete measurements of other elements has given the impression that the collapsed element was subjected to deviations in its cover. These points combined indicate that the failed grandstand element in the stadium was likely subjected to large variations in the concrete cover. The three presented reliability assessments have shown that the collapse of the element in the Goffert stadium cannot be explained by the actually occurred loads being higher than the design loads, but rather by a weaker than intended resistance of the element resulting from execution errors in the concrete cover and the positioning of the main reinforcement.

6   Conclusions

In this paper a probabilistic forensic assessment on the collapsed element in the Goffert stadium was performed. Stochastic variables related to jump type loads were quantified. These variables were used to generate excitation signals. The following conclusions can be drawn from this study:

- When using the structural properties resulting from the design drawings, the assessment was unable to explain why the collapsed element failed with such a high probability. The proposed dynamical model, combined with a state of the art excitation signal and a resistance function as intended based on technical drawings give no cause for the very large observed failure probability.

- Concrete cover measurements of other elements combined with the sensitivity of the post-yielding capacity to the structure's reliability make it more plausible that the actual structure was weaker than intended, rather than the actual loads being higher than the design loads.

While this paper developed a novel method to perform a probabilistic forensic assessment on a collapsed grandstand element, there are still areas for improvement and future research. The following are recommendations for future work:

- The influence human structure interaction has on the response needs further investigation. In particularly, the interaction between a group of people and the structure should be explored.
- The choice of damping parameters is a critical factor in determining the structure's response, making the present model conservative. In this paper, damping due to hysteresis was assumed to be negligibly small which is also conservative. Further work can be carried out to obtain reliable parameters which would improve the model's accuracy.
- The probabilistic model in this paper was intended to find a most likely cause for failure in a forensic assessment. The method can be extended to a reliability based calibration of design loads in order to establish the jumping load value coupled to a certain required reliability level. So the current paper does not deal with the question which design loads to use but deals only with the question of the failure cause.

References

A. Ebrahimpour, R.L. Sack. Modeling dynamic occupant loads. In: *Journal of Structural Engineering* 115.6 (1989), pp. 1476–1496.

A. Tsouvalas, P. Ditmar. Structural Response to Earthquakes. Reader of course CIE5260, Delft University of Technology, Faculty of Civil Engineering and Geosciences, 2020.

B.R. Ellis, T. Ji. Loads generated by jumping crowds: experimental assessment. In: BRE information paper IP 4, BRE publishing (2002).

B.R. Ellis, T. Ji. Loads generated by jumping crowds: numerical modelling. In: *Structural Engineer* 82.17 (2004), pp. 35–40.

B.R. Ellis, T. Ji, J.D. Littler. The response of grandstands to dynamic crowd loads. In: *Proceedings of the Institution of Civil Engineers-Structures and Buildings* 140.4 (2000), pp. 355– 365.

C. Gaspar, E. Caetano, C. Moutinho, J.G. Santos da Silva. Active human-structure interaction during jumping on floors. In: *Structural Control and Health Monitoring* 27.3 (2020).

E. Shahabpoor, A. Pavic. Human-structure dynamic interaction during short-distance free falls. In: *Shock and Vibration* 2016 (2016).

Eurocode 1: Actions on structures – Part 1-1: General actions – Densities, self-weight, imposed loads for buildings. Standard: European Committee for Standardization, Nov. 2007.

H. Bachmann, W. Ammann. Vibrations in structures: induced by man and machines. Vol. 3. *IABSE*, 1987.

H. Schlune, M. Plos, K. Gylltoft. Safety formats for non-linear analysis of concrete structures. In: *Magazine of Concrete Research* 64.7 (2012), pp. 563–574.

International Standard ISO 10137: Bases for design of structures - Serviceability of buildings and walkways against vibrations. Standard. International Organization for Standardization, Nov. 2007.

J.M.W. Brownjohn, A. Pavic, P. Omenzetter. A spectral density approach for modelling continuous vertical forces on pedestrian structures due to walking. In: *Canadian Journal of Civil Engineering* 31.1 (2004), pp. 65–77.

J. Chen, H. Tan, K. van Nimmen, P. van den Broeck. "Data-driven synchronization analysis of a bouncing crowd". In: *Shock and Vibrion* 2019 (2019).

J. R. Casas, D.F. Wisniewski, J. Cervenka, V. Cervenka, R. Pukl, E. Bruwhiler, A. Herwig, G. Holm, M. Olsson, P.E. Bengtsson, M. Plos, Safety and Probabilistic Modelling: Sustainable Bridges Background document D4. 4. 2007.

V. Racic, J.M.W. Brownjohn, and A. Pavic. 2010. Reproduction and application of human bouncing and jumping forces from visual marker data." *J. Sound Vib*. 329 (16): 3397–3416.

J. Sim, A. Blakeborough, M.S. Williams, G. Parkhouse. "Statistical model of crowd jumping loads". In: *Journal of structural engineering* 134.12 (2008), pp. 1852–1861.

Loading for buildings Part 1. Code of practice for dead and imposed loads. Standard. British Standard, Sept. 1996.

M.V. Sivaselvan, A.M. Reinhorn. Hysteretic models for cyclic behavior of deteriorating inelastic structures. Multidisciplinary Center for Earthquake Engineering Research Buffalo, NY, 1999.

M. Spanenburg. Dynamische belasting op tribunes. In: *Cement* 2 (2022), pp. 36–46.

National Building Code of Canada 2005 Volume 1. Standard. Canadian Commission on Building and Fire Codes, 2005.

Royal HaskoningDHV. Onderzoek naar de technische oorzaken van het bezwijken van het tribune-element van het Goffert stadion te Nijmegen. Gemeente Nijmegen, Feb. 2022.

S. Yao, Jr. Wright, A. Pavic, P. Reynolds. Forces generated when bouncing or jumping on a flexible structure. In: *Proceedings of the international conference on noise and vibration*. Vol. 2. 2002, pp. 563–572.

T. Ji, B.R. Ellis. Floor vibration induced by dance-type loads: theory. In: *Structural Engineer* 2 (1994), pp. 37–37.

Trillingen van vloeren door lopen. Standard. SBR, Sept. 2005.

J. Xiong, J. Chen. Open access and updated human-induced load data set. In: *Journal of Structural Engineering* 147.3 (2021), p. 04720003.